Magnetic local time asymmetries in electron and proton precipitation with and without substorm activity

Olesya Yakovchuk[1,2] and Jan Maik Wissing [1]

[1]The Institute of Environmental Systems Research, University of Osnabrück, Osnabrück, 49069, Germany
[2]Skobeltsyn Institute of Nuclear Physics, Lomonosov Moscow State University, Moscow 119234, Russia

Correspondence: Olesya Yakovchuk (oyakovchuk@uos.de)

Abstract. The magnetic local time (MLT) dependence of electron (0.15–300 keV) and proton (0.15–6900 keV) precipitation into the atmosphere based on National Oceanic and Atmospheric Administration POES and METOP satellites data during 2001–2008 was described. Using modified APEX coordinates the influence of particle energy, substorm activity and geomagnetic disturbance on the MLT flux distribution was statistically analysed.

5 Some of the findings are: a) MLT flux differences of up to $1:2^5$ have been localized inside the auroral oval. b) MLT dependence can be assigned to different particle sources and energy-specific drifts. c) The maximum flux asymmetry ratio depends on particle energy, but not necessarily on geomagnetic disturbance. For protons it is invariant with Kp, for electrons the dependence varies with Kp and kinetic energy defines how. c) Substorms mostly increase particle precipitation in the night-sector by about factor 2–4 but can also reduce it in the day-sector.

10 Finally we have a look at MLT-dependent trapped particle flux in the plasmasphere, which shows vast and abstract MLT differences.

1 Introduction

Particle precipitation is the main link between solar activity and atmospheric chemistry. Thorne (1977) suggested a depletion of Ozone in 40–80 km through production of nitric oxides by precipitation of relativistic radiation belt electrons. Ozone depletion

15 following solar energetic particle events (mostly protons) has been observed in the same year (Heath et al., 1977). Auroral particle precipitation is due to production and downwelling of HO_y a significant player in mesospheric and stratospheric chemistry, especially as it catalytically impacts the ozone cycle (Callis et al., 1996b, a) and subsequently changes the radiation budget and affects dynamics. Consequently there has been an immanent need for the description (and later on modelling) of the particle precipitation. And even though the investigation of precipitation pattern of low energetic particles (and especially

20 electrons) started more then 30 years ago (Hardy et al., 1985, e.g.), the rising vertical extend of climate models has shifted the focus from high energetic particles to lower energies again.

  The interplanetary medium is the driver of geomagnetic disturbance and may compress, deform or reconnect to the magnetosphere. Meredith et al. (2011) e.g. states that on average, the flux of precipitating energy electrons (E>30 keV) is enhanced

by a factor of about 10 during the passage of the high-speed stream (geomagnetic storm time) at all geographic longitudes. Thus geomagnetic disturbance should be considered in a description of particle precipitation.

Magnetic local time dependence is a result of charge-dependent drift directions (Allison et al., 2017) and (linked to that) opposite potentials in field-aligned Birkeland-currents. The authors themselves note that the particle flux variety in different

5   local time sectors may reach an order of magnitude, with proton precipitation dominating in evening and night sectors and electrons dominating in morning and night (Wissing et al., 2008).

Substorms are either directly driven or/and loading processes, where energy is accumulated and released abruptly in the Earth's magnetosphere (Akasofu, 2015). The global morphology of auroral substorms has first been described by Akasofu (1964) using simultaneous all-sky camera recordings from Siberia, Alaska and Canada. Later space-born missions like e.g. the

10 UV photometer mission on Dynamics Explorer 1 (DE-1) (Frank et al., 1981) confirmed this morphology.

Akasofu et al. (1965) also already characterized the expansion phase and the recovery phase of a substorm (a preceding growth phase has been added by McPherron (1970)). Due to auroral emissions the substorms were associated with excitation and ionization by precipitating particles that have been investigated by ground based riometers (Berkey et al., 1974) and later on by satellite missions (e.g. Fujii et al., 1994), observing intense energetic electron precipitation in or near the onset/surge

15 region. The energy range of the precipitating particles has been defined as electrons and protons at approx. 10–100keV with a low-energy cut-off (Birn et al., 1997). The precipitation regions depend on particle species.

The occurrence of substorms depends on the orientation of the interplanetary magnetic field (Reeves et al., 2003). As shown in Reeves et al. (2003) these external solar wind parameters subsequently impact the magnetic field on the ground and are represented in the AE index. In this study we use the SML index to define substorm onsets, which is the lower envelope of

20 the SME, an index derived likewise to the AE but based on all available magnetometer stations in these latitudes (Newell and Gjerloev, 2011a).

In this study we will discuss MLT differences in particle precipitation on a wide energy range and show how substorms impact this pattern.

In Section 2 particle data, modified APEX coordinate system, SML and Kp-binning will be introduced. Section 3 displays

25 the application of modified APEX coordiantes to the precipitation maps. In Section 4 and 5 we will analyse the particle precipitation on high latitudes and low latitudes, respectively. The results are summarized in Section 6.

2   Data sets

This section describes the data sets and how the data has been processed.

2.1   Particle data

30 For particle precipitation we use time series (2001–2008) of 16 s averaged electron fluxes ranging from 0.15 to 300 keV and protons from 0.15 to 6900 keV measured on board the polar orbiting NOAA/POES and their successor, the MetOp satellites (Evans and Greer, 2006). 2001 to 2008 covers the complete declining phase of solar cycle 23 and thus includes very active

Table 1. Channels from the POES and METOP satellites which have been used.

	instrument	channel	energy range
electrons	TED	band 4	154–224 eV
		band 8	688–1000 eV
		band 11	2.115–3.075 keV
		band 14	6.503–9.457 keV
	MEPED	mep0e1-e2	30–100 keV
		mep0e2-e3	100–300 keV
protons	TED	band 4	154–224 eV
		band 8	688–1000 eV
		band 11	2.115–3.075 keV
		band 14	6.503–9.457 keV
	MEPED	mep0P1	30–80 keV
		mep0P2	80–240 keV
		mep0P3	240–800 keV
		mep0P4	0.8–2.5 MeV
		mep0P5	2.5–6.9 MeV

(sometimes extreme) to very low activity periods. Information about the different channels can be found in Tab. 1. In total all
available data from POES 15, 16, 17, 18 and MetOp 02 has been used, except for POES 16 after 2006 as it is known that the
TED data is erroneous.

All satellites have sun-synchronous orbits at altitudes around 820 km (with ≈ 100 minute periods of revolution) and an inclination of ≈ 98.5°. The satellites have initially been placed in orbits that cross the equator in a fixed local time either being morning-evening or day-night sector. However, or in our case furtunately, these orbits were drifting slightly with time. Thus our long sample period and the moving five satellites allowed us to investigate the effect of local time on particle precipitation.

5   It should be said that the particle detectors suffer from various contamination effects:

The MEPED electron channels are highly efficient detectors for high energetic protons. In order to avoid contaminated electron data we excluded MEPED electrons when the omnidirectional proton channel P7 showed more than 2 counts (based on high resolution 2 s data). This does not only cut out probably contaminated periods in SPEs, but also the region of the SAA. The MEPED electron channels have been substracted from each other, resulting in differential channels.

10   It is known that there is no adequate upper energy threshold of the three MEPED electron channels (Yando et al., 2011). In order to work with specific energy bands we subtracted sequent channels, resulting in the two channels mep0e1-e2 and mep0e2-e3 with the energy bounds given in Tab. 1.

It should be mentioned that we used the 0° detectors only. While the TED 0°-detector looks exactly radially outward the MEPED 0°-detector is slightly shifted by 9° to ensure a clear field of view (Evans and Greer, 2006). In high latitudes both

15   detectors count precipitating particle flux while they detect trapped particles in low latitudes.

2.2 Coordinate system

A meaningful representation of particle precipitation has high requirements for the coordinate system as they are: a) The precipitation pattern should be invariant in time even though the magnetic field is changing (meaning moving poles, not magnetospheric distortion). This is needed for the long investigation period as well as for durability of forecasts. b) The

20   latitude of particle precipitation should be invariant of the longitude. Given this criterion the longitude may be replaced by local time as second coordinate. c) If the previous criterion is applied, it includes that particle flux has to be recalculated. Following the footpoints of two shells with a distinct magnetic field strength, their latitudinal distance differs with longitude. Since the particle flux is measured on a fixed detector size this has to be taken into account when removing the longitudinal dependence. d) Particle measurements take place at the position of the satellite, which is in about 820 km above the ground.

25   But the effect of particle precipitation (the atmospheric ionization) is mainly located in about 110 km altitude (maximum of magnetospheric ionization, higher particle energies cause ionization futher down). Consequently a coordinate system that allocates the satellite's measurement to their respective position at 110 km altitude would be helpful.

The coordinate system that allows for all named requirements is the modified APEX coordinate system (Richmond, 1995). The coordinates are variable in time using the International Geomagnetic Reference Field model magnetic field configuration,

30   which means they also reflect the temporal movement of the poles. Richmond (1995) present three coordinate systems which are closely connected. The quasi-dipole coordinates present the magnetic latitude and longitude on the ground (Richmond, 1995, see f1 and f2 base vectors in Fig. 1), while the third base vector goes radially outward. The APEX coordinate system is using the same longitude, but the latitude is following the magnetic field lines as propagating (precipitating) particles do, meaning that a charged particle is always on the same latitude. The APEX latitude is defined by its footpoint on the QD latitude

on the surface. In the *modified* APEX coordinates not the surface but an arbitary altitude is used for the definition of the latitude, e.g. that altitude where particles cause the ionization, in our case 110 km above the ground. Thus the measurements should be mapped down on the according field line until it reaches the altitude where the particle is stopped by the atmosphere (about 110 km). In all (modified) APEX systems measurements and ionization location are on the same latitude. Thus a desirable

5   coordinate system for our work is the modified APEX system.

2.3   SML index and derived substorm onsets

The period 2001–2008 was chosen for our investigation, where all necessary data about substorms and particle precipitation are available. For the identification of substorm events, we use the technique published by Newell and Gjerloev (2011a). The substorm onset is determined by the auroral electrojet SML index, which is derived from magnetometer data obtained by the

10   SuperMAG magnetometer network. The SuperMAG magnetometer network in the northern hemisphere (up to 100 stations) improves the traditional auroral electrojet (AL) network (12 stations) (Newell and Gjerloev, 2011a).

Newell and Gjerloev (2011b) distinguish recurrent and isolated substorms. While recurrent substorms appear in groups with less than 82 min between their onsets, the isolated substorm onsets are separated by at least 3 h. Only the isolated substorms are used in our investigation, as this helps to avoid two or more substorms overlapping each other. Contrasting the isolated

15   substorm periods we also use time periods without any substorms (no-substorm period). The total number of substorm onsets for our period constitutes 15 316 events. Defining 30 min after an onset as typical length of a substorm, we end up with 10.4% of the whole period being generally substorm-influenced (while the rest is no-substorm). However, just 1.87% of the whole period can be attributed to isolated substorms.

It should be noted that with this technique we are not able to separate different substorm phases nor can we distinguish dif-

20   ferent types of substorms. Independend from substorm phase, the proton aurora is displaced equatorward of the electron aurora for dusk local times, and it is poleward for dawn local times. In the onset region however, proton and electron precipitation depends on the substorm phase and may even be colocated (Mende et al., 2003). Thus the results represent a mean substorm value.

2.3.1   Kp-binning of particle data

25   The Kp-index is a three-hourly index estimating the geomagnetic activity (Bartels et al., 1939). In contrast to the AL/SML index which describes the auroral electrojet activity, the Kp-index is sensitive to several current systems (e.g. the ring current) and thus describes the magnetospheric activity with a more global perspective.

The particle data has been binned into three Kp-level groups. These levels have been chosen in a way that each bin contains approx. the same amount of 3-hour periods: Kp 0–1 (quiet): 7660, Kp 1.3-2.3 (less quiet): 7666 and Kp 2.7-9 (unsettled to

30   storm): 8050. This sums up to the 8 year period. However, as the amount of satellites is not constant, the substorms are not evenly distributed in time and the local time sectors are not evenly covered, single data points (with 1 h MLT-resolution, 2 degrees latitudinal resolution and the Kp-binning) may contain a different amount of the 16 s averages.

3 Precipitation map

Binning of particle flux strongly depends on the coordinate system. Some features are determined by the inner magnetic field and thus co-rotating with Earth, while others are influenced by the interaction with the solar wind and according to that fixed in relation to the Sun and to the (magnetic) local time. Since we will use the modified APEX coordinates in this paper we will

5 have a look how the particle flux representation differs to geographic coordinates and which aspects can be best described in the two systems.

Figure 1 shows the TED proton band 11 in geographic and modified APEX 110 km coordinates. No selection according to Kp-level or substorm intensity has been made, while all available data from MetOP 2 and POES 15, 16, 17 and 18 for the years 2001–2008 has been included.

10 Most obvious in the geographic representation is the South Atlantic Anomaly (SAA, located roughly between -70 and 0 degrees East and -45 to 0 degrees North). Being a dip in the geomagnetic field, the SAA allows energetic particles in the radiation belt to reach altitudes low enough to be reached by the satellite's orbit. Thus the high flux values are not necessarily connected to high particle precipitation. As the SAA is a geomagnetic feature it is co-rotating and thus best represented in the geographic coordinates, while a MLT based coordinate system intermixes SAA patterns with non SAA patterns on the same

15 latitude.

A feature that is connected to the SAA is the particle precipitation in the drift loss cone. Particles drift around Earth and bounce between the mirror points. These mirror points get to lowest altitudes where the magnetic field is weakest. Since the geomagnetic field around the SAA is weak the dominating particle precipitation zone is where these field lines have their foot points. In Fig. 1 (upper panel) this can be clearly identified South-East of the SAA. In the northern hemisphere the particle

20 precipitation due to the drift loss cone is less dominant, but still visible.

Apart from that the geographic representation is not very helpful. Due to the satellites' inclination the poles are not covered and typical pattern as the auroral precipitation is meandering.

Switching to magnetic coordinates (here: modified APEX 110 km) straightens the auroral oval and mostly removes the longitudinal dependence (not shown). Consequently we can replace the APEX longitude by MLT (see Fig. 1, lower panel).

25 Of cause the SAA and the drift loss cone are now smeared out (see e.g. double auroral structure) and still produce a hemispheric asymmetry, but features that depend on the local time now become visible and the auroral oval itself does not show a hemispheric dependence.

Most obvious in the modified APEX/MLT coordinates are the local time dependencies in the auroral zone as well as in lower latitudes. Substorm depended precipitation that mostly appears during night time can also be identified (see following

30 sections).

Some regions in modified APEX/MLT coordinates will never be reached as the local time coverage is limited. This holds for the midnight hours in the northern hemisphere as well as for noon in low latitudinal Southern hemisphere. The equatorial region seems not to be covered, however, is not a data gap. The flux is mapped to the latitude where the guiding field-line hits
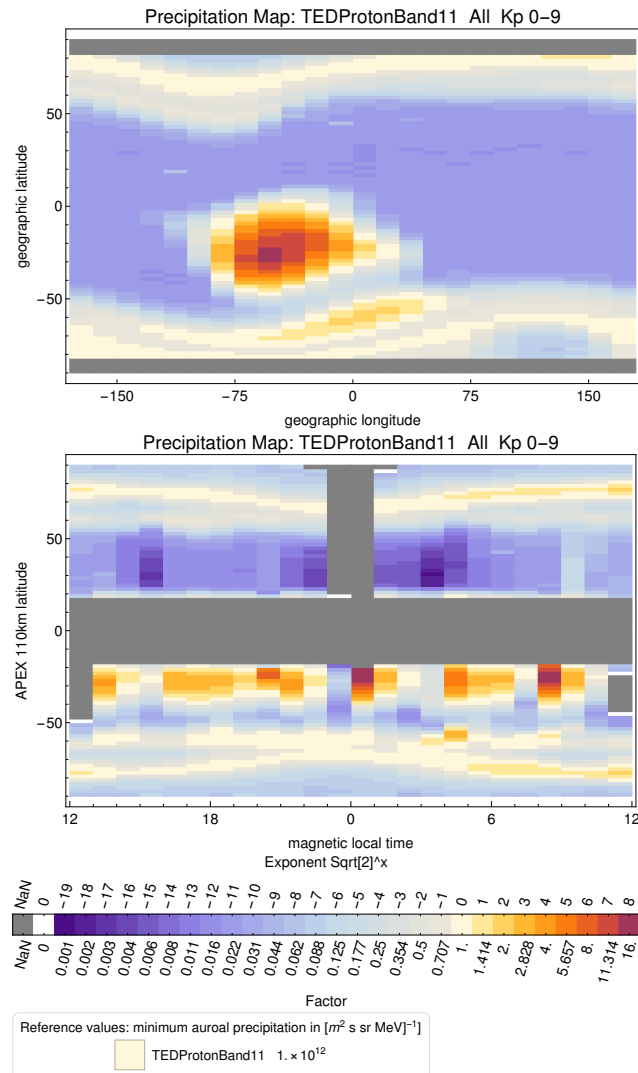
Figure 1. Particle flux in the TED proton band 11 in geographic and modified APEX 110 km coordinates. The color scale marks the minimum flux in the auroral oval in beige. The neighbouring color indicates that the flux is a factor $\sqrt{2}$ apart (the neighbour after that a factor 2).

110 km. Since the satellites cross the (dip) equator at 850 km all field lines peak below that point are not covered (<19 degrees N/S). Since the magnetic poles are shifted to the geographic ones the satellites' inclination does not limit the polar coverage.

As a consequence of the regional coverage and SAA influence we will select the Southern hemisphere auroral zone and the low latitudes in Northern hemisphere for further investigation.

4   High Latitudes

Figure 2 shows the precipitating electron flux in high latitudes in the southern hemisphere. The southern hemisphere has been chosen to avoid the data gaps between 23 and 1 MLT in the northern hemisphere (see the Section 5). Apart from that, northern and southern hemisphere do not show significant differences in APEX coordinates.

5   The color scale is logarithmic with a base of two, meaning the threshold to the adjacent color is a factor of 2 apart. The reference value has been set individually for every channel to the lowest occurring value inside the auroral oval. Thus local time differences can be easily identified and quantified. No-substorm periods (left panel) and isolated substorm periods (right panel) for all electron channels are given here.

Comparing these two panels of Fig. 2, we can identify:

10   1. Generally, the main **precipitation zone** (white to reddish colours) **moves equatorward with increasing particle energy**.

 2. Quantitatively, the particle precipitation shows distinct MLT dependence. The range of this dependence changes with particle energy. While the two **lowest TED electron channels (band 4 and 8) show just minor MLT variations, in the higher particle energies it varies by more than one order of magnitude**.

   During isolated **substorms** the maximum local time **differences are similar or a factor of 2 higher** (and the maximum
15   is located in the midnight sector during substorms, see next paragraph). For details and a summary of other (not shown) Kp-bins, see Table 2.

 3. Qualitatively, MLT variations also depend on particle energy:

   (a) The **higher particle channels** (above >2 keV) **show a movement of the main precipitation with MLT from midnight** (TED electron band 11) **via morning sector** (mep0e1-e2corr) **to day sector** (mep0e2-e3corr). An expla-
20   nation for the movement in the higher electron channels (and the opposite directed movement of the protons) is the westward partial ring current in the night side which is closed by flied-aligned currents (Birkeland Region 2) into the ionosphere (Lockwood, 2013; Milan et al., 2017). While electrons in ring current drift eastwards and thus may precipitate predominantly in the morning sector, the protons undergo a westward drift and mainly precipitate in the evening sector. The energy dependence might be due to different drift velocities (Allison et al., 2017). A drift of
25   electron precipitation (>20 keV) towards the dayside has also been reported by Matthews et al. (1988); Newell and Meng (1992); Østgaard et al. (1999) and is associated with central plasmasheet electron injections in the midnight region. The resulting dawn-dusk asymmetry for electrons also depends on Kp-level.

   The maximum **MLT-asymmetry depends on Kp: for the low energetic channels** band 4 and 8 **it decreases** with Kp, in band 11 it stays the same but **for** the **more energetic** band 14, mep0e1-e2 and mep0e2-e3 (where it shows a
30   clear dawn-dusk asymmetry) **it increases with Kp**. In the Kp-bins chosen for our study it doubles from bin to bin (see Table 2). And even for Kp 0–1 the dawn-dusk asymmetry stays visible with a factor of about 2 to 4 in TED electron band 14 and mep0e1-e2 (not shown but same pattern as in Fig. 2).
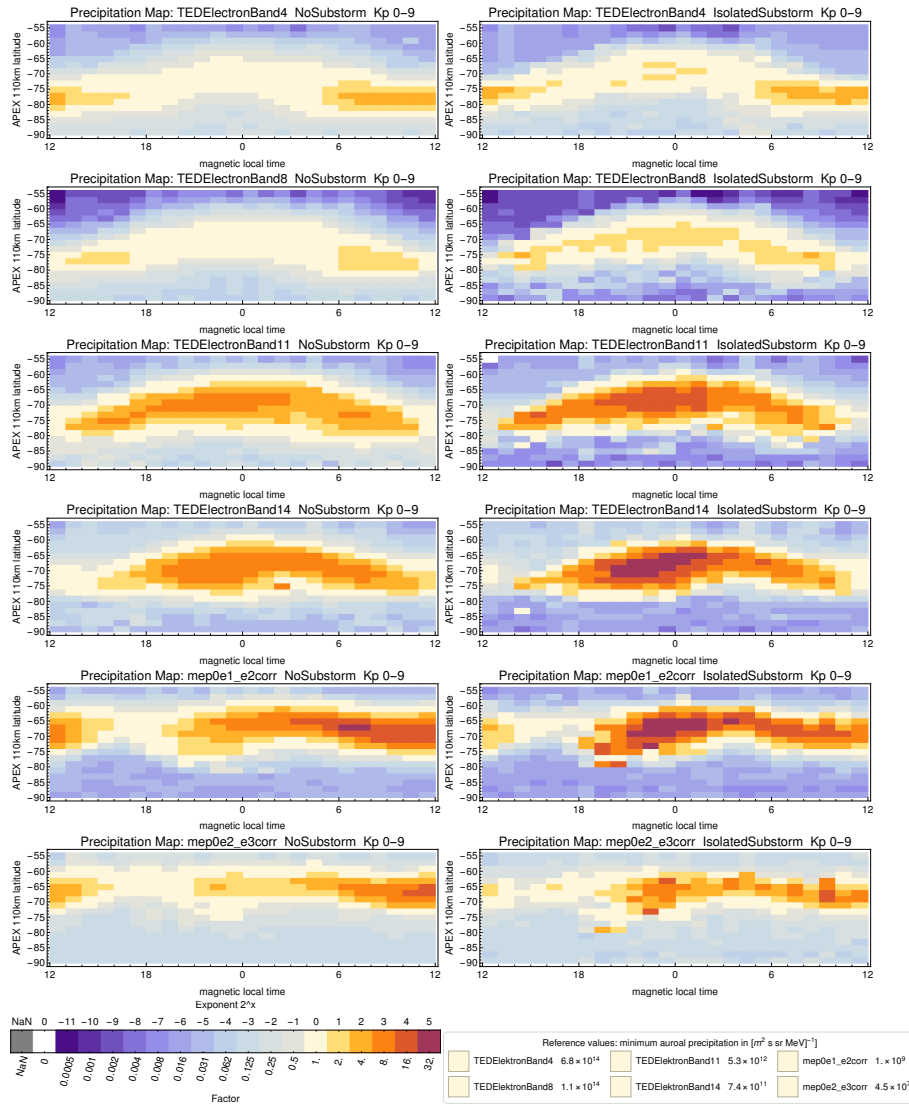
Figure 2. Electron flux in various channels in high latitudes on the southern hemisphere. Left panel shows periods without substorms, right panel gives periods with isolated substorms only.

For isolated **substorms the movement is** the same, but **superimposed with** substorm-specific **night-side** (20–2 MLT) **particle precipitation** which reflects the substorm electrojet manifestations (Lockwood, 2013; Milan et al., 2017). The electron precipitation intensity at midnight sector outnumbers the no-substorm values at the same place by factor 2 to 4. For mep0P1 to mep0P3 the evening sector is slightly increased during substorms.

5   (b) The **lower TED electron band 4 and 8 peak between 6 and 17 MLT**. Since this is completely opposite to the higher channels we will have a look at the source region.

The main precipitation of low energetic electrons (<1 keV) at daytime (e.g. 76–80 S, 6–13 MLT for TED electron band 4) most likely origins from the poleward edge of the cusp, referring to Sandholt et al. (1996); Øieroset et al. (1997); Sandholt et al. (2000) who attribute this as source region during periods with northward IMF (which in our

10   study mostly refers to no-substorm periods as southward IMF triggers substorms). In contrast, during periods with isolated substorms the precipitation is shifted by 2 degrees to the equator (the shift can be identified throughout TED electron bands 4 and 8). The source in this case is the equatorward edge of the cusp which has been identified as corresponding source region in periods of southward IMF by Sandholt and Newell (1992); Sandholt et al. (1998). A sketch including the source regions may be found in Newell and Meng (1992, Fig. 2), even though the regions

15   are labled with Mantle and Cusp here.

(c) Additionally it can be noticed that **noon sector electron fluxes decrease during a substorm**, which is clearly seen in all upper channels (from TED electron band 11 to mep0e2-e3).

(d) An **increasing dusk-dawn asymmetry with substorm activity** (as e.g. Allison et al. (2017) noted for trapped radiation belt electrons) **cannot be identified**. In contrast, it seems that substorm activity simply adds particle

20   precipitation in the night side and reduces high energetic electron precipitation around noon.

Figure 3 shows the same as Figure 2 but for protons. Comparing no-substorm periods (left panel) with isolated substorm periods (right panel) as well as with the electron precipitation from Figure 2, we can identify:

1. The **protons also show an equatorward movement of the main precipitation zone with increasing particle energy**.

2. **Low energetic protons** (TED proton band 4–14) **show a second oval structure** (approx. 50–65 S), which is associated

25   with the drift loss cone (see the Section 3) and thus geographically localized near the SAA. The second oval structure itself is a artifact of the MLT-binning (see Fig. 1).

3. Quantitatively, the **proton particle precipitation shows distinct MLT dependence**, ranging from just **minor variations in TED proton band 11 and 14** (as well as **no MLT variation in the highest MEPED channels**) up to about **one order of magnitude in the lowest and medium particle energies** (TED proton band 4 and 8, MEPED mep0P1 and mep0P3).

30   During isolated substorms the maximum local time differences are similar or a factor of 2 higher (see Table 2).

4. In contrast to the electrons the **maximum asymmetry of protons does not depend on Kp**-index.

5. Qualitatively:
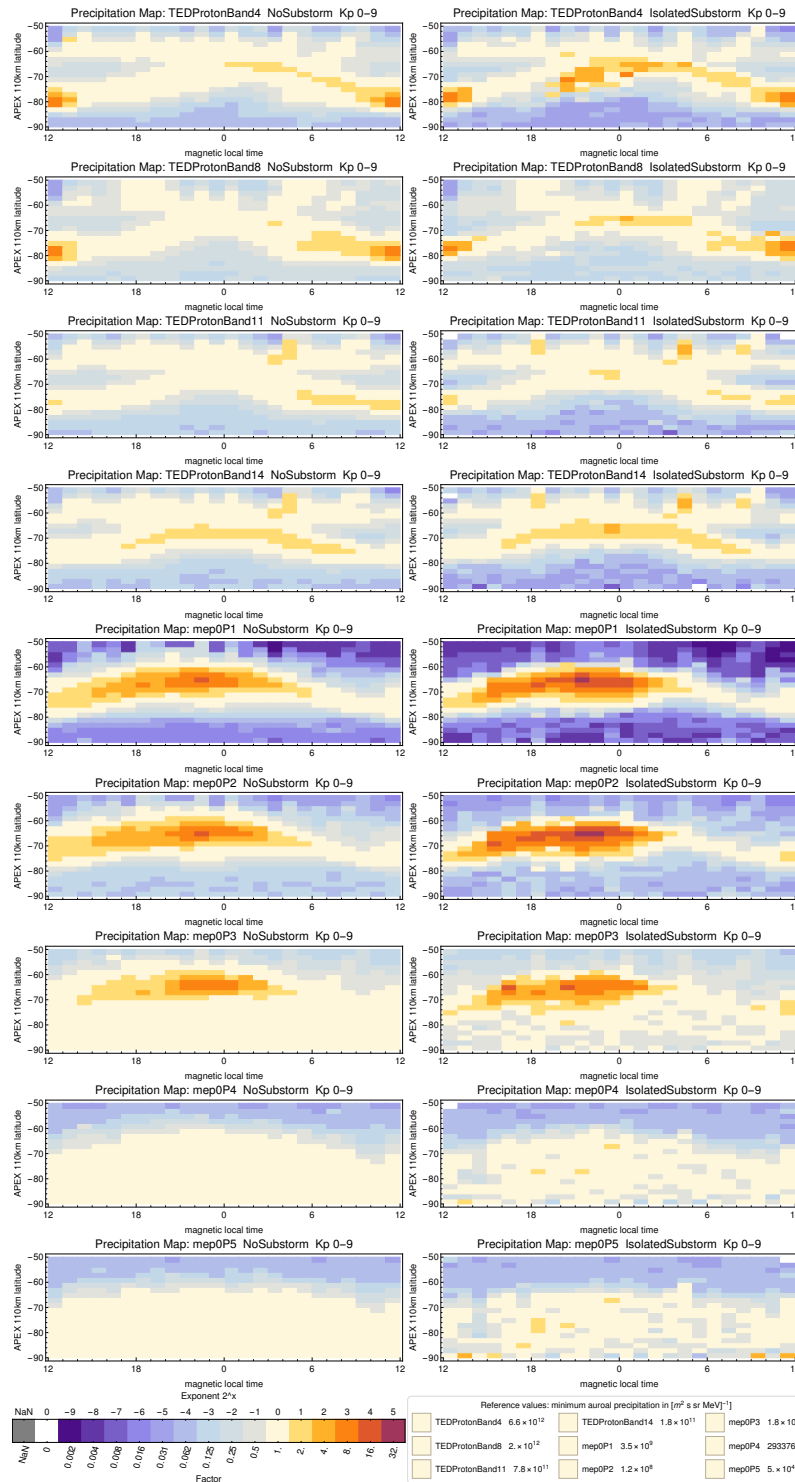
Figure 3. Proton flux in various channels in high latitudes on the southern hemisphere.

(a) **Low energetic proton precipitation** (no-substorm) is **mostly concentrated around noon**. Additionally there is a slight increase from noon via the morning sector towards midnight.

The precipitation **during isolated substorms is shifted to lower latitudes** by about 2 degrees. Since we have seen a similar picture for low energetic electrons (see description to Figure 2, Paragraph 3b) we conclude that during no-substorm periods the particles originate from the poleward edge of the cusp, while during isolated substorms they originate from the equatorward edge of the cusp.

(b) Between TED proton band 14 and the following channels (mep0P1 to mep0P3) the **main particle precipitation zone moves from midnight to the evening sector**, which is oppositely directed to the electron movement. The possible explanation has already been given in the description to Figure 2 (Paragraph 3a).

(c) The two **highest energy channels** (MEPED mep0P4 and mep0P5) **do not show MLT variations**. Particle precipitation is limited to solar proton events. Since these particles enter the ionosphere via open field lines there is no latitudinal focussing but a homogeneous precipitation within the polar cap.

(d) Regarding the effect of **substorm** events, the **proton precipitation intensity at midnight sector outnumbers the no-substorm values** at the same place by factor 2 to 4.

(e) In contrast to the electron fluxes the **day sector proton fluxes do not significantly depend on substorm** activity.

5   Low Latitudes

Fig. 1 (lower panel, $24°$–$52°$N[1]) also revealed another obviously MLT-dependent pattern, which cannot be attributed to direct particle precipitation as in low latitudes the $0°$ (radially outward looking) detector measures particles that gyrate around their guiding field line with a high pitch angle. Thus we see a mostly trapped particle population here. Given that all Kp-bins show a similar MLT-pattern independently from substorm activity it seems worth mentioning – even though particle flux itself is small, not connected with precipitation and raising a couple of questions.

Figure 4 is a close-up of the described region and shows particle flux in low latitudes in the Northern hemisphere. The northern hemisphere has been chosen to exclude the SAA.

Our aim is to depict the MLT variations and how some of them might be explained.

Fig. 4 reflects the limited local time coverage, even though up to five satellites have been used in an 8 year period. The missing two local time bins from 23–1 h are marked in gray.

The color scale is logarithmic to a base of two, meaning the threshold to an adjacent colour is a factor of 2 apart. The reference value has been set individually for every channel to the lowest occurring value. Thus MLT differences can be easily identified and quantified. It should be noted that only no-substorm periods and just one of the probed Kp-levels is given here.

---

[1]Converting the modified APEX 110 km longitude into geographic longitude, the lower boundary is between 4.2 and $24.0°$ N while the upper boundary is between 39.6 and $55.8°$ N.

Table 2. Exponent to the base 2 between lowest and highest flux in the auroral oval.

Channel	Kp 0–1	1.3–2.3	2.7–9	0–9	
	no	no	no	no	sub
proton band 4	4	3	3	3	3
proton band 8	3	3	3	3	3
proton band 11	1	1	2	1	2
proton band 14	1	1	1	1	2
mep0P1	3	3	3	4	5
mep0P2	4	4	4	4	5
mep0P3	2	3	3	3	4
mep0P4	0	0	0	0	1
mep0P5	0	0	0	0	1
electron band 4	3	3	2	2	2
electron band 8	2	1	1	1	2
electron band 11	3	3	3	3	4
electron band 14	3	4	5	3	5
mep0e1-e2	3	4	5	5	5
mep0e2-e3	2	3	4	4	4

The relations during isolated substorm periods are given for Kp 0-9

(meaning all isolated substorms) only to avoid bad statistics.

Acronyms: sub=substorm, no=no-substorm.

The reason is that there is no distinct difference to substorm periods (except for worse statistics) and no significant difference to other Kp-levels as well.

Our findings are:

1. **Typical for electron and proton TED bands is a flux minimum around midnight.** For the lowest channel, band 4 (electron and proton), it is centered at midnight (20–4 MLT), for the higher TED channels it appears shifted to the morning sector centered around 2 or 3 MLT. While the general picture can be explained by the primary particle source being the sunlit ionosphere, which also justifies that the strongest day-night asymmetry is seen in the very low energetic channels, which are (or are close to) the thermal spectrum, the MLT-shift for higher energies remains unclear.

2. The **highest** electron (mep0e2-e3) and proton **channels** (mep0P2, mep0P3, mep0P4 and mep0P5) **do not show MLT-variations** in low latitudes. Since one reason for it has already been explained as these channels are far from the thermal source population another reason is given by Allison et al. (2017), who also investigated trapped electrons and explained
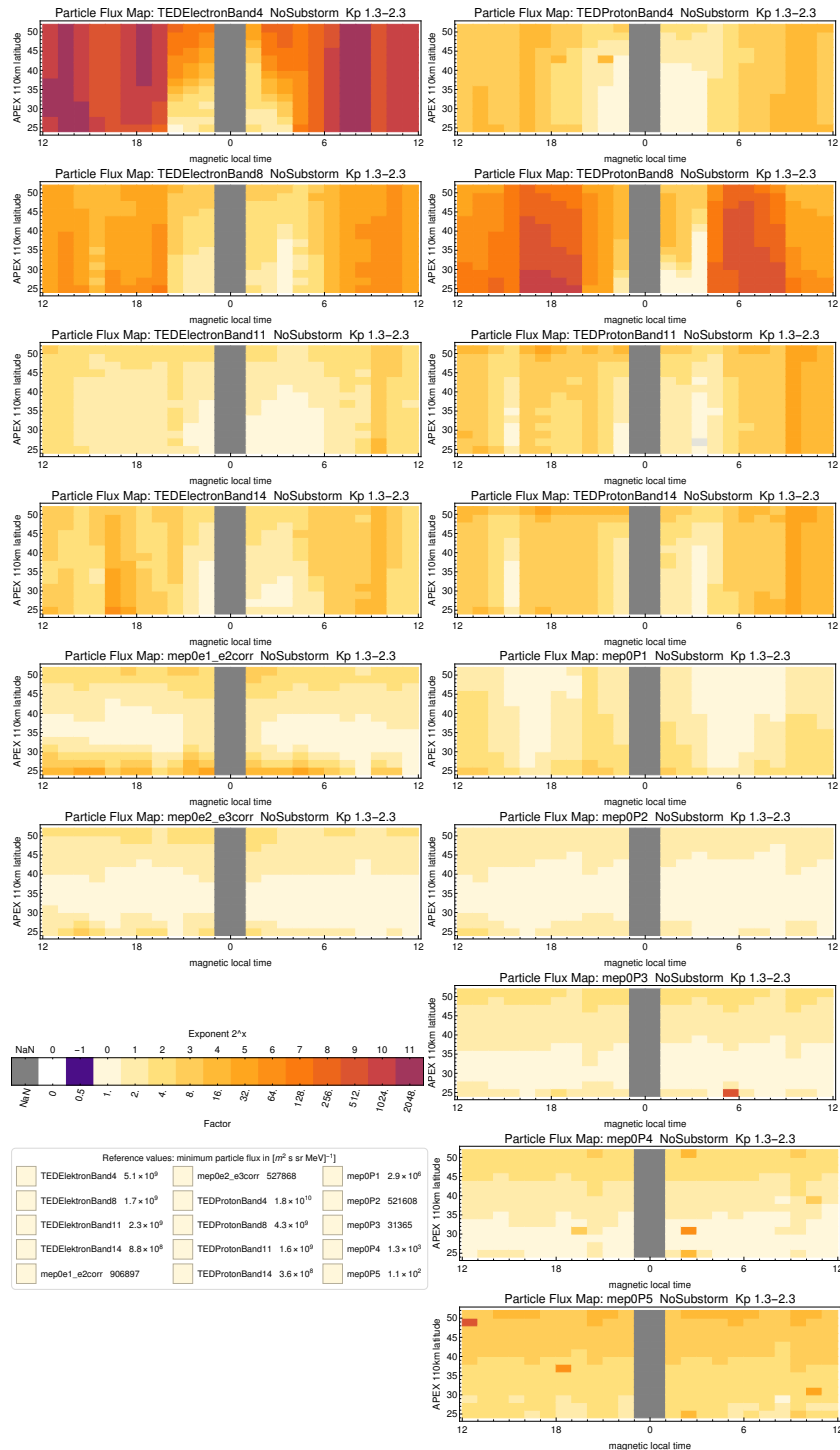
Figure 4. Relative particle flux in various channels in low latitudes on the Northern hemisphere in relation to the lowest occuring flux value. Gray indicates missing data around midnight.

Table 3. MLT flux difference at low latitudes. Maximum relative difference between flux measurements on the same latitude is presented. Please note that not ratio but its exponent to the base of two is given, meaning that the highest MLT-flux difference for protons (in proton band 8) is a factor $2^{11} = 2048$.

Channel	relative difference (exponent to 2^x)
proton band 4	4
proton band 8	11
proton band 11	5
proton band 14	5
mep0P1	3
electron band 4	11
electron band 8	6
electron band 11	4
electron band 14	6
mep0e1-e2	2

the decreasing MLT-dependence with energy by higher drift velocity of high energetic particles that (in combination with closed drift paths) result in more uniform MLT patterns.

3. **At 14-16 MLT** however, **a local minimum can be found** in 5 channels (electron band 4, 8 and 14 and proton band 11 and 14) probably even in mep0P1, but then shifted by +2 MLT. The reason might be plasmaspheric plumes that are capable of transporting particles from the plasmasphere to the dusk sector of the dayside outer magnetosphere (Borovsky et al., 2013; Chen and Moore, 2006; Walsh et al., 2014) and which often occur in this MLT range.

Aspects that remain unclear but also can be identified in all Kp-bins are:

4. **Medium** electron and proton **channel** (mep0e1-e2 and mep0P1) **show a flux maximum around midnight** in contrast to the lower channels that have a local minimum here. It might also be that the midnight-minimum moved to the morning sector. However, the flux difference is just about a factor of 2 to 4, which is significantly less than in the low energetic channels.

5. A phenomena that can be identified in at least 6 channels (electron band 8, 11 and 14 and proton band 4, 11 and 14) is **a local flux maximum from 9-10 MLT**. It seems like a counter-part of the plasmaspheric plume since it is located in the same MLT distance to noon but on the morning sector. However, it is not known that something like a counter-part of the plasmaspheric plume exists. Consequently the reason for this flux enhancement is not known to the authors.

6 Summary

In this paper we presented the MLT-distribution of energetic particle precipitation into the ionosphere in combination with different substorm activity as well as MLT-dependent trapped particle flux in the plasmasphere.

Concerning the precipitating particles we could identify different particle sources for low and high energetic particles. Different sources and energy-specific drifts lead to MLT-dependence of the dominating precipitation: < 1 keV in the day-sector (protons concentrated at noon), above a few keV in the night-sector. Above that the charge-dependent drift clearly separates electron and proton precipitation. With increasing electron energy electrons move via morning-sector to the day-sector, while the main proton precipitation moves to the evening sector with a maximum at about 22 MLT.

Also quantitatively the MLT-variation depends on energy: with a few 100 eV the relatively focussed peak at noon produces a medium asymmetry (exponent 2–3). With slightly higher energies that vanishes and the asymmetry declines (exponent 1–2). As soon as the (partial) ring current becomes dominant the asymmetry peaks (exponent up to 5). For higher energies (just protons available) the asymmetry breaks down to zero.

While the MLT-variation is invariant in Kp for protons, the MLT-asymmetry for electrons depends on geomagnetic disturbance. For low energetic electrons < 1 keV it declines with Kp and for electron > 6 keV it increases with Kp.

The effect of substorms is mostly limited to the night-sector, where it generally enhances particle precipitation. For electrons the day-sector also is affected, where electron precipitation declines (seen for 2–300 keV). For medium energy protons (30–800 keV) the evening sector is slightly increased. Quantitatively, isolated-substorm periods enhance the flux in the night sector by approx. factor 2 to 4, while the day-sector decrease might be up to factor 2. Consequently the resulting MLT-differences enlarge during substorms.

MLT-dependency at low latitudes are regarded even though they are not linked to particle precipitation, but because they show a) extreme asymmetries (up to a ratio of 1:2000), which can be attibuted to the particle source of the plasmasphere, being the sunlit thermosphere and b) because one MLT-region shows a depletion which might be due to a plasmaspheric plume. However, some of the MLT-features at low latitudes still raise questions.

Competing interests. The authors declare that they have no conflict of interest.

Acknowledgements. The authors acknowledge the NOAA National Centers for Environmental Information (https://ngdc.noaa.gov/stp/satellite/poes/dataaccess.html) for the POES and METOP particle data used in this study and give many thanks to the SuperMAG team (http://supermag.jhuapl.edu/) and their collaborators (http://supermag.jhuapl.edu/info/?page=acknowledgement).
The work is supported by the DFG project WI4417/2-1.

References

Akasofu, S.-I.: The development of the auroral substorm, Planet. Space Sci., 12, 273–282, https://doi.org/10.1016/0032-0633(64)90151-5, 1964.

Akasofu, S.-I.: Auroral substorms as an electrical discharge phenomenon, Progress in Earth and Planetary Science, 2, 20, https://doi.org/10.1186/s40645-015-0050-9, 2015.

Akasofu, S. I., Chapman, S., and Meng, C. I.: The polar electrojet, Journal of Atmospheric and Terrestrial Physics, 27, 1275–1300, https://doi.org/10.1016/0021-9169(65)90087-5, 1965.

Allison, H. J., Horne, R. B., Glauert, S. A., and G., D.: The magnetic local time distribution of energetic electrons in the radiation belt region, J. Geophys. Res. Space Physics, 122, 20, https://doi.org/doi:10.1002/2017JA024084, 2017.

Bartels, J., Heck, N. H., and Johnston, H. F.: The three-hour-range index measuring geomagnetic activity, Terrestrial Magnetism and Atmospheric Electricity, 1939.

Berkey, F. T., Driatskiy, V. M., Henriksen, K., Hultqvist, B., Jelly, D. H., Shchuka, T. I., Theander, A., and Ylindemi, J.: A synoptic investigation of particle precipitation dynamics for 60 substorms in IQSY (1964-1965) and IASY (1969), Planetary and Space Science, 22, 255–307, https://doi.org/10.1016/0032-0633(74)90028-2, 1974.

Birn, J., Thomsen, M. F., Borovsky, J. E., Reeves, G. D., McComas, D. J., and Belian, R. D.: Characteristic plasma properties during dispersionless substorm injections at geosynchronous orbit, J. Geophys. Res., 102, 2309–2324, https://doi.org/10.1029/96JA02870, 1997.

Borovsky, J. E., Denton, M. H., Denton, R. E., Jordanova, V. K., and Krall, J.: Estimating the effects of ionospheric plasma on solar wind/magnetosphere coupling via mass loading of dayside reconnection: Ion-plasma-sheet oxygen, plasmaspheric drainage plumes, and the plasma cloak, Journal of Geophysical Research: Space Physics, 118, 5695–5719, https://doi.org/10.1002/jgra.50527, https://agupubs.onlinelibrary.wiley.com/doi/abs/10.1002/jgra.50527, 2013.

Callis, L. B., Baker, D. N., Natarajan, M., Bernard, J. B., Mewaldt, R. A., Selesnick, R. S., and Cummings, J. R.: A 2-D model simulation of downward transport of NO_y into the stratosphere: Effects on the 1994 austral spring O_3 and NO_y, Geophys. Res. Lett., 23, 1905–1908, https://doi.org/10.1029/96GL01788, 1996a.

Callis, L. B., Boughner, R. E., Baker, D. N., Mewaldt, R. A., Bernard Blake, J., Selesnick, R. S., Cummings, J. R., Natarajan, M., Mason, G. M., and Mazur, J. E.: Precipitating electrons: Evidence for effects on mesospheric odd nitrogen, Geophys. Res. Lett., 23, 1901–1904, https://doi.org/10.1029/96GL01787, 1996b.

Chen, S.-H. and Moore, T. E.: Magnetospheric convection and thermal ions in the dayside outer magnetosphere, Journal of Geophysical Research: Space Physics, 111, https://doi.org/10.1029/2005JA011084, https://agupubs.onlinelibrary.wiley.com/doi/abs/10.1029/2005JA011084, 2006.

Evans, D. S. and Greer, M. S.: Polar Orbiting Environmental Satellite Space Environment Monitor - 2, Instrument Descriptions and Archive Data Documentation, NOAA Space Environ. Lab, Boulder, Colo, USA, 2006.

Frank, L. A., Craven, J. D., Ackerson, K. L., English, M. R., Eather, R. H., and Carovillano, R. L.: Global auroral imaging instrumentation for the Dynamics Explorer Mission, Space Science Instrumentation, 5, 369–393, 1981.

Fujii, R., Hoffman, R. A., Anderson, P. C., Craven, J. D., Sugiura, M., Frank, L. A., and Maynard, N. C.: Electrodynamic parameters in the nighttime sector during auroral substorms, J. Geophys. Res., 99, 6093–6112, https://doi.org/10.1029/93JA02210, 1994.

Hardy, D. A., Gussenhoven, M. S., and Holeman, E.: A statistical model of auroral electron precipitation, J. Geophys. Res., 90, 4229–4248, https://doi.org/10.1029/JA090iA05p04229, 1985.

Heath, D. F., Krueger, A. J., and Crutzen, P. J.: Solar proton event - Influence on stratospheric ozone, Science, 197, 886–889, https://doi.org/10.1126/science.197.4306.886, 1977.

Lockwood, M.: Reconstruction and Prediction of Variations in the Open Solar Magnetic Flux and Interplanetary Conditions, Living Reviews in Solar Physics, 10, 4, https://doi.org/10.12942/lrsp-2013-4, 2013.

5 Matthews, D. L., Rosenberg, T. J., Benbrook, J. R., and Bering, III, E. A.: Dayside energetic electron precipitation over the South Pole (lambda = 75 deg), Journal of Geophysical Research, 93, 12 941–12 945, https://doi.org/10.1029/JA093iA11p12941, 1988.

McPherron, R. L.: Growth phase of magnetospheric substorms, J. Geophys. Res., 75, 5592, https://doi.org/10.1029/JA075i028p05592, 1970.

Mende, S. B., Frey, H. U., Morsony, B. J., and Immel, T. J.: Statistical behavior of proton and electron auroras during substorms, Journal of Geophysical Research (Space Physics), 108, 1339, https://doi.org/10.1029/2002JA009751, 2003.

10 Meredith, N. P., Horne, R. B., Lam, M. M., Denton, M. H., Borovsky, J. E., and Green, J. C.: Energetic electron precipitation during high-speed solar wind stream driven storms, Journal of Geophysical Research (Space Physics), 116, A05223, https://doi.org/10.1029/2010JA016293, 2011.

Milan, S. E., Clausen, L. B. N., Coxon, J. C., Carter, J. A., Walach, M.-T., Laundal, K., Østgaard, N., Tenfjord, P., Reistad, J., Snekvik, K., Korth, H., and Anderson, B. J.: Overview of Solar Wind-Magnetosphere-Ionosphere-Atmosphere Coupling and the Generation of

15 Magnetospheric Currents, Space Science Rev., 206, 547–573, https://doi.org/10.1007/s11214-017-0333-0, 2017.

Newell, P. T. and Gjerloev, J. W.: Evaluation of SuperMAG auroral electrojet indices as indicators of substorms and auroral power, Journal of Geophysical Research (Space Physics), 116, A12211, https://doi.org/10.1029/2011JA016779, 2011a.

Newell, P. T. and Gjerloev, J. W.: Substorm and magnetosphere characteristic scales inferred from the SuperMAG auroral electrojet indices, Journal of Geophysical Research (Space Physics), 116, A12232, https://doi.org/10.1029/2011JA016936, 2011b.

20 Newell, P. T. and Meng, C.-I.: Mapping the dayside ionosphere to the magnetosphere according to particle precipitation characteristics, Journal of Geophysical Research, 19, 609–612, https://doi.org/10.1029/92GL00404, 1992.

Øieroset, M., Sandholt, P. E., Denig, W. F., and Cowley, S. W. H.: Northward interplanetary magnetic field cusp aurora and high-latitude magnetopause reconnection, Journal of Geophysical Research, 102, 11 349–11 362, https://doi.org/10.1029/97JA00559, 1997.

Østgaard, N., Stadsnes, J., Bjordal, J., Vondrak, R. R., Cummer, S. A., Chenette, D. L., Parks, G. K., Brittnacher, M. J., and McKenzie, D. L.:

25 Global-scale electron precipitation features seen in UV and X rays during substorms, Journal of Geophysical Research, 104, 10 191–10 204, https://doi.org/10.1029/1999JA900004, 1999.

Reeves, G. D., Henderson, M. G., Skoug, R. M., Thomsen, M. F., Borovsky, J. E., Funsten, H. O., C:son Brandt, P., Mitchell, D. J., Jahn, J.-M., Pollock, C. J., McComas, D. J., and Mende, S. B.: IMAGE, POLAR, and Geosynchronous Observations of Substorm and Ring Current Ion Injection, in: Disturbances in Geospace: The Storm-substorm Relationship, edited by Surjalal Sharma, A., Kamide, Y., and Lakhina,

30 G. S., vol. 142 of *Washington DC American Geophysical Union Geophysical Monograph Series*, p. 91, https://doi.org/10.1029/142GM09, 2003.

Richmond, A. D.: Ionospheric Electrodynamics Using Magnetic Apex Coordinates., Journal of Geomagnetism and Geoelectricity, 47, 191–212, https://doi.org/10.5636/jgg.47.191, 1995.

Sandholt, P. E. and Newell, P. T.: Ground and satellite observations of an auroral event at the cusp/cleft equatorward boundary, Journal of

35 Geophysical Research, 97, 8685–8691, https://doi.org/10.1029/91JA02995, 1992.

Sandholt, P. E., Farrugia, C. J., Øieroset, M., Stauning, P., and Cowley, S. W. H.: Auroral signature of lobe reconnection, Geophysical Research Letters, 23, 1725–1728, https://doi.org/10.1029/96GL01846, 1996.

Sandholt, P. E., Farrugia, C. J., Moen, J., and Cowley, S. W. H.: Dayside auroral configurations: Responses to southward and northward rotations of the interplanetary magnetic field, Journal of Geophysical Research, 103, 20 279–20 296, https://doi.org/10.1029/98JA01541, 1998.

Sandholt, P. E., Farrugia, C. J., Cowley, S. W. H., Lester, M., Denig, W. F., Cerisier, J.-C., Milan, S. E., Moen, J., Trondsen, E., and Lybekk,
5   B.: Dynamic cusp aurora and associated pulsed reverse convection during northward interplanetary magnetic field, Journal of Geophysical Research, 105, 12 869–12 894, https://doi.org/10.1029/2000JA900025, 2000.

Thorne, R. M.: Energetic radiation belt electron precipitation - A natural depletion mechanism for stratospheric ozone, Science, 195, 287–289, https://doi.org/10.1126/science.195.4275.287, 1977.

Walsh, A. P., Haaland, S., Forsyth, C., Keesee, A. M., Kissinger, J., Li, K., Runov, A., Soucek, J., Walsh, B. M., Wing, S., and Taylor, M.
10   G. G. T.: Dawn–dusk asymmetries in the coupled solar wind–magnetosphere–ionosphere system: a review, Annales Geophysicae, 32, 705–737, https://doi.org/10.5194/angeo-32-705-2014, https://www.ann-geophys.net/32/705/2014/, 2014.

Wissing, J. M., Bornebusch, J., and Kallenrode, M.-B.: Variation of energetic particle precipitation with local magnetic time, Advances in Space Research, 41, 1274–1278, https://doi.org/10.1016/j.asr.2007.05.063, 2008.

Yando, K., Millan, R. M., Green, J. C., and Evans, D. S.: A Monte Carlo simulation of the NOAA POES Medium Energy Pro-
15   ton and Electron Detector instrument, Journal of Geophysical Research: Space Physics, 116, https://doi.org/10.1029/2011JA016671, https://agupubs.onlinelibrary.wiley.com/doi/abs/10.1029/2011JA016671, 2011.